TITLE

Hsf1 phosphorylation generates cell-to-cell variation in Hsp90 levels and promotes phenotypic plasticity

AUTHORS

Xu Zheng[1,*], Ali Beyzavi[2,5,*], Joanna Krakowiak[1], Nikit Patel[3], Ahmad S. Khalil[3,4,#], David Pincus[1,#,§]

[1] Whitehead Institute for Biomedical Research, Cambridge, USA

[2] Department of Mechanical Engineering, Boston University, Boston, USA

[3] Department of Biomedical Engineering and Biological Design Center, Boston University, Boston, USA

[4] Wyss Institute for Biologically Inspired Engineering, Harvard University, Boston, USA

[5] Present address: Koch Institute for Integrative Cancer Research, Cambridge, USA

* These authors contributed equally

[#] Correspondence: khalil@bu.edu, pincus@wi.mit.edu

[§] Lead contact: pincus@wi.mit.edu

ABSTRACT

Clonal populations of cells exhibit cell-to-cell variation in the transcription of individual genes. In addition to this “noise” in gene expression, heterogeneity in the proteome and the proteostasis network expands the phenotypic diversity of a population. Heat shock transcription factor (Hsf1) regulates chaperone gene expression, thereby coupling transcriptional noise to proteostasis. Here we show that cell-to-cell variation in Hsf1 activity is an important determinant of phenotypic plasticity. Budding yeast cells with high Hsf1 activity were enriched for the ability to acquire resistance to an antifungal drug, and this enrichment depended on Hsp90 – a known “phenotypic capacitor” and canonical Hsf1 target. We show that Hsf1 phosphorylation promotes cell-to-cell variation, and this variation – rather than absolute Hsf1 activity – promotes antifungal resistance. We propose that Hsf1 phosphorylation enables differential tuning of the proteostasis network in individual cells, allowing populations to access a wide range of phenotypic states.

INTRODUCTION

Genetically identical cells grown together in the same environment nonetheless display cell-to-cell variation in gene expression (Colman-Lerner et al., 2005; Elowitz et al., 2002; Raser and O'Shea, 2004, 2005; Weinberger et al., 2005). While most frequently observed in microorganisms, such as bacteria and yeast, gene expression variation is also found in developing mammalian cells and human embryonic stem cells (Silva and Smith, 2008; Stelzer et al., 2015). Such variation has been proposed to be the mechanistic underpinning of lineage commitment during human development, the epithelial to mesenchymal transition in cancer metastasis, organ regeneration in planarians, bacterial persistence in the presence of antibiotics, and the ability of yeast cells to remain fit in fluctuating environments (Harms et al., 2016; Newman et al., 2006; Oderberg et al., 2017; Silva and Smith, 2008; Ye and Weinberg, 2015). While differences in cell size, cell cycle position and chromatin state can partially account for cell-to-cell variation, much of the variability has been attributed to the inherently stochastic process of gene expression (Colman-Lerner et al., 2005; Raj and van Oudenaarden, 2008; Raser and O'Shea, 2005). Despite the underlying stochasticity, gene expression variation itself varies widely across the genome, with some sets of genes showing very low variation among cells (e.g., ribosomal protein genes) and other sets of genes (e.g., stress responsive genes) showing high levels of variation (Newman et al., 2006). Yet, individual genes within these regulons show strong covariance, indicating the source of the variation lies in the activity of upstream transcription factors and signaling pathways (Stewart-Ornstein et al., 2012). As such, cell-to-cell variation may be a property that is under genetic control and can be tuned up and down over evolution.

On top of this gene expression variation, cell-to-cell differences also exist in the state of the proteome. Perhaps the most striking examples of proteome variation come from prion proteins, which can exist in either soluble or self-templating amyloid conformations (Shorter and

61 Lindquist, 2005). Prions have been shown to have the ability to broadly reshape the proteome
62 by challenging chaperones and other components of the protein homeostasis (proteostasis)
63 machinery and even by globally altering protein translation (Serio and Lindquist, 1999; Shorter
64 and Lindquist, 2008). Moreover, chaperones themselves can exist in large heterotypic
65 complexes that differ between cells in what has been termed the “epichaperome,” giving rise to
66 altered susceptibility of cancer cells to drugs that target the essential chaperone Hsp90 (Rodina
67 et al., 2016). By buffering the proteome and stabilizing near-native protein folds, Hsp90 has
68 been shown to mask latent genetic variation in fruit flies and plants and to enhance the ability of
69 yeast cells to acquire novel phenotypes such as resistance to anti-fungal drugs (Cowen and
70 Lindquist, 2005; Queitsch et al., 2002; Rutherford and Lindquist, 1998). In this regard, Hsp90
71 has been termed a “phenotypic capacitor” (Sangster et al., 2004).
72
73 Heat shock factor 1 (Hsf1) regulates the expression of many components of the proteostasis
74 machinery – including Hsp90 – in eukaryotes from yeast to humans (Anckar and Sistonen,
75 2011). In unstressed budding yeast cells, a different chaperone, Hsp70, binds to Hsf1 and
76 restrains its activity. Upon heat shock, Hsp70 dissociates from Hsf1 leaving Hsf1 free to induce
77 expression of its target genes (Zheng et al., 2016). Heat shock also triggers Hsf1 hyper-
78 phosphorylation. Although phosphorylation is a conserved hallmark of Hsf1 activation, it is
79 dispensable for acute Hsf1 activity during heat shock. Rather than switching Hsf1 on,
80 phosphorylation enables Hsf1 to sustain increased activity during prolonged exposure to
81 elevated temperature (Zheng et al., 2016). Here we identify a novel role for Hsf1 – and Hsf1
82 phosphorylation – that may have provided a strong selective advantage during evolution. We
83 show that Hsf1 generates cell-to-cell variation in Hsp90 levels, which in turn contributes to the
84 ability of *Saccharomyces cerevisiae* to acquire resistance to the antifungal drug fluconazole. We
85 find that the ability of Hsf1 to become phosphorylated is a key factor in generating population

86 level heterogeneity in its activity. We propose that by coordinately controlling cytosolic
87 chaperone genes including Hsp90, Hsf1 promotes phenotypic plasticity.
88
89 **RESULTS**
90 **Differential cell-to-cell variation in Hsf1 activity in response to heat shock and AZC**
91 In addition to heat shock, Hsf1 is known to respond to a variety of chemical stressors that impair
92 proteostasis. In particular, the small molecule azetidine 2-carboxylic acid (AZC) is known to
93 strongly activate Hsf1 (Trotter et al., 2002). AZC is a proline analog that is charged onto $tRNA^{pro}$
94 and incorporated into nascent proteins during translation, impairing their subsequent folding
95 (Fowden and Richmond, 1963). Our previous mass spectrometry data indicated that Hsf1
96 displays distinct phosphorylation patterns in cells that had been heat shocked compared to cells
97 treated with AZC (Zheng et al., 2016). To explore these differences, we monitored
98 phosphorylation of FLAG-tagged Hsf1 following heat shock and treatment with AZC by
99 observing its electrophoretic mobility over time by western blot. Heat shock induced progressive
100 and sustained Hsf1 phosphorylation leading to a dramatic shift in its mobility over the heat
101 shock time course (Figure 1A). By contrast, AZC led to only a modest shift in Hsf1 mobility
102 (Figure 1A). Despite these differences in phosphorylation, both heat shock and AZC robustly
103 induced Hsf1 transcriptional activity as measured by flow cytometry of cells expressing HSE-
104 YFP, a fluorescent reporter of Hsf1 transcriptional activity (Figure 1B) (Zheng et al., 2016).
105 While heat shock resulted in rapid HSE-YFP induction, plateauing after 1 hour, AZC induced
106 Hsf1 activity with delayed but sustained kinetics, ultimately leading to the same maximal output
107 level as heat shock after 4 hours (Figure 1B).
108
109 Along with altered activation kinetics, we observed differences in the single cell fluorescence
110 distributions: the populations of cells that had been heat shocked showed a broad distribution of
111 HSE-YFP levels, while cells treated with AZC showed narrower distributions, indicating reduced

levels of cell-to-cell variation in Hsf1 activity. To account for potential differences in cell size, we normalized each cell's HSE-YFP fluorescence by its size as measured by side scatter (SSC) and plotted the resulting normalized distributions over the heat shock and AZC time courses (Figure 1C, D) (Stewart-Ornstein et al., 2012). Direct comparison of the HSE-YFP/SSC distributions following 4 hours of heat shock or treatment with AZC reveals that despite a slightly higher average level of Hsf1 activation in the AZC-treated cells, cellular heterogeneity is greatly reduced compared to heat shocked cells (Figure 1E). To quantify this cell-to-cell variation in the HSE-YFP reporter, we calculated the square of the coefficient of variation (CV^2) (Stewart-Ornstein et al., 2012). While the CV^2 drops as the mean increases for both heat shocked and AZC-treated cells, it is 3-fold higher in heat-shocked cells by the end of the experiment (Figure 1F). These data show that while heat shock and AZC both potently activate Hsf1, they do so with distinctive features. Heat shock triggers rapid Hsf1 activation coupled to high levels of phosphorylation and results in a high degree of cell-to-cell variation in the HSE-YFP reporter. By contrast, AZC induces slow, sustained Hsf1 activation, modest Hsf1 phosphorylation and reduced noise in the HSE-YFP reporter.

Hsf1 phosphorylation generates cell-to-cell variation during heat shock

Since increased Hsf1 phosphorylation was associated with increased cell-to-cell variation in the HSE-YFP reporter, we wondered if Hsf1 phosphorylation was responsible for increasing noise during heat shock. To test this, we leveraged a non-phosphorylatable mutant we had previously generated, $Hsf1^{\Delta po4}$, in which we mutated all 152 possible sites of phosphorylation to alanine (Zheng et al., 2016). We performed a heat shock time course and measured the HSE-YFP reporter by flow cytometry in wild type cells and cells expressing $Hsf1^{\Delta po4}$. Indeed, after normalizing for cell size, we observed reduced noise in the HSE-YFP reporter in the $Hsf1^{\Delta po4}$ cells compared to wild type throughout the heat shock time course (Figure 2A, B). As an orthogonal approach to measure cell-to-cell variation in Hsf1 activity, we developed a

138 microfluidic-based assay to measure the HSE-YFP reporter in single cells over time in response
139 to heat shock using a novel platform that enables precision temperature control (Figure 2C,
140 Figure S1). In agreement with the flow cytometry data, cells expressing Hsf1$^{\Delta po4}$ showed lower
141 noise in HSE-YFP levels over the heat shock time course (Figure 2D, E). Thus, Hsf1
142 phosphorylation promotes cell-to-cell variation in Hsf1 activity during heat shock.
143
144 **Hsp90 expression displays Hsf1-dependent cell-to-cell variation**
145 To investigate functional roles for cell-to-cell variation in Hsf1 activity, we monitored expression
146 of Hsp90, an endogenous Hsf1 target gene known to influence phenotypic plasticity (Cowen
147 and Lindquist, 2005). Budding yeast encodes two Hsp90 paralogs, Hsc82 and Hsp82, with
148 Hsc82 being highly expressed under all conditions and Hsp82 showing both basal and inducible
149 expression in response to heat shock (Solis et al., 2016). We tagged Hsp82 with YFP and
150 monitored its expression in single cells expressing either wild type Hsf1 or Hsf1$^{\Delta po4}$ by
151 fluorescence microscopy and flow cytometry. Consistent with the HSE-YFP reporter, Hsp82-
152 YFP expression showed greater variability among wild type cells than Hsf1$^{\Delta po4}$ cells (Figure 3A,
153 B).
154
155 Prior studies have implicated Hsp90 as a “phenotypic capacitor” that promotes the ability of cells
156 to acquire novel phenotypes (Sangster et al., 2004). In particular, in fungi, Hsp90 has been
157 shown to increase the rate at which cells acquire resistance to the anti-fungal drug fluconazole
158 (Cowen and Lindquist, 2005). We hypothesized that the increased cell-to-cell variation in
159 Hsp82-YFP expression levels in wild type cells compared to Hsf1$^{\Delta po4}$ cells would translate into
160 increased fluconazole resistance. Indeed, wild type cells generated significantly more
161 fluconazole resistant colonies than Hsf1$^{\Delta po4}$ cells (Figure 3C, D).
162
163 **Acquired fluconazole resistance is enriched in cells with high Hsf1 activity**

164 Since noise in Hsp82-YFP levels and the HSE-YFP reporter correlated with phenotypic
165 plasticity, we wondered if individual cells with elevated HSE-YFP levels would be more likely to
166 become resistant to fluconazole. To test this, we used fluorescence activated cell sorting
167 (FACS) to isolate the tails of the HSE-YFP distribution – the 10% of cells with the highest and
168 lowest HSE-YFP expression levels – in wild type cells, *hsp82Δ* and *hsc82Δ* cells (Figure 3E). In
169 wild type cells, the tail with high HSE-YFP expression was enriched for fluconazole resistant
170 colonies over the low expression tail (Figure 3F). By contrast, the high expression tails of the
171 *hsp82Δ* and *hsc82Δ* cells showed no enrichment, with the *hsc82*Δ high expression tail actually
172 showing decreased resistance (Figure 3F). These results indicate that cells with higher levels of
173 Hsf1 activity have an increased ability to acquire resistance to an antifungal drug, and this ability
174 depends on Hsp90.
175
176 **Fluconazole resistance correlates with variation in Hsf1 activity, not its magnitude**
177 Since the high expression tail of the HSE-YFP distribution was enriched for cells able to acquire
178 resistance to fluconazole, we hypothesized that if we could increase the average HSE-YFP
179 expression, we could increase the ability of cells to acquire fluconazole resistance. To test this,
180 we expressed wild type Hsf1 from a promoter under the control of a synthetic, estradiol-
181 responsive (ER) transcription factor (Zheng et al., 2016). In this way, we could titrate the amount
182 of estradiol to tune the expression level of Hsf1, and thereby control the expression level of its
183 target genes and the HSE-YFP reporter. In parallel, we also expressed $Hsf1^{\Delta po4}$ using the same
184 system to determine if the deficit in cell-to-cell variation could be overcome by increasing the
185 absolute expression (Figure 4A). We grew the wild type and $Hsf1^{\Delta po4}$ cells in a dilution series of
186 estradiol, maintained growth at $OD_{600} < 0.5$ for 18 hours and measured the HSE-YFP reporter.
187 Estradiol induced dose-dependent induction of the HSE-YFP in both wild type and $Hsf1^{\Delta po4}$
188 cells, though with a steeper curve for $Hsf1^{\Delta po4}$ cells (Figure 4B, C). At all doses of estradiol, wild
189 type had higher CV^2 in the HSE-YFP reporter than $Hsf1^{\Delta po4}$ cells (Figure 4B, D). We tested the

190 ability of cells expressing wild type Hsf1 and Hsf1$^{\Delta po4}$ at low (1 nM), medium (8 nM) and high (32
191 nM estradiol) levels to acquire resistance to fluconazole (Figure 4E). Surprisingly, increasing
192 median HSE-YFP did not increase resistance: both wild type and Hsf1$^{\Delta po4}$ cells showed maximal
193 resistance at low Hsf1 expression (Figure 4F). However, wild type cells showed greater
194 resistance at all Hsf1 expression levels than Hsf1$^{\Delta po4}$ cells (Figure 4F). Thus, increased variation
195 in HSE-YFP levels – not increased median levels – positively correlates with fluconazole
196 resistance (Figure 4G-I).
197
198 **DISCUSSION**
199 Cell-to-cell variation in gene expression and the state of the proteome have been proposed to
200 contribute to adaptability in populations of genetically identical cells. Here we identify a single
201 regulatory mechanism that couples variation at the transcriptional and proteomic levels:
202 phosphorylation of the transcription factor Hsf1. We found that when wild type Hsf1 is activated
203 and concomitantly hyperphosphorylated – as is the case during heat shock – cells display high
204 variation in their expression of downstream Hsf1 target genes. By contrast, when Hsf1 is
205 activated without hyperphosphorylation following treatment with AZC, cells show more uniform
206 target gene expression. Moreover, removing the ability of Hsf1 to be phosphorylated reduced
207 cell-to-cell variation. Since the Hsf1 regulon consists of chaperones and other proteostasis
208 factors, variation in Hsf1 activity is likely to lead to variation in the proteostasis network and the
209 state of the proteome.
210
211 Functionally, we demonstrated that cell-to-cell variation in Hsf1 activity is correlated with the
212 ability of cells to acquire resistance to the antifungal drug fluconazole, in large part via
213 expression of the known phenotypic capacitor Hsp90. While wild type cells with high levels of
214 Hsf1 activity were enriched for the ability to acquire fluconazole resistance, cells with reduced
215 levels of Hsp90 lost this enrichment. This observation suggested that cells with more Hsf1

activity would have more Hsp90 and therefore show increased antifungal resistance. However, synthetically increasing Hsf1 activity resulted in diminished fluconazole resistance. Moreover, increased expression of non-phosphorylatable Hsf1$^{\Delta po4}$ – which showed reduced cell-to-cell variation in its activity compared to wild type Hsf1 – could not compensate for its reduced ability to support fluconazole resistance. Thus, antifungal resistance correlates with variation in Hsf1 activity rather than with the magnitude of Hsf1 activity.

How does Hsf1 phosphorylation lead to cell-to-cell variation and why does variation promote fluconazole resistance? It is likely that differential activation of cell cycle, metabolic and stress responsive kinase pathways results in differential Hsf1 phosphorylation states and leads to distinct levels of transcriptional activity in single cells. However, the finding that variation in Hsf1 activity rather than its absolute activity drives resistance is more intriguing. Although cells with synthetically elevated Hsf1 activity produce more Hsp90, they also overproduce the rest of the Hsf1 regulon, which may be maladaptive. In addition, with forced Hsf1 activity, cells are unable to dynamically regulate Hsf1 to precisely tune its activity according to need. While a high level of Hsf1 activity – and thus Hsp90 levels – may be beneficial early in the process of acquiring resistance to fluconazole, it may be that a subsequent reduction in Hsf1 activity promotes proliferation. The capacity for dynamic and coordinated control over the proteostasis network may endow cells with the plasticity required to maintain fitness in fluctuating environments. By enabling both population-level variation and dynamic control over the proteostasis network, Hsf1 is a powerful phenotypic capacitor.

ACKNOWLEDGEMENTS

We dedicate this paper to Susan Lindquist and her scientific legacy. We are grateful to K. Reynolds and R. Ranganathan for beneficial discussions, to the Whitehead Institute FACS facility for technical assistance and to N. Azubuine and T. Nanchung for a constant supply of plates and media. This work was supported by an NIH Early Independence Award (DP5 OD017941-01 to D.P.) and a National Science Foundation CAREER Award (MCB-1350949 to A.S.K.).

AUTHOR CONTRIBUTIONS

Conceptualization, D.P. and A.S.K; Methodology, X.Z., A.B. N.P.; Investigation, X.Z., A.B., J.K., D.P., N.P.; Writing, D.P. and A.S.K; Funding Acquisition, D.P. and A.S.K.; Supervision, D.P. and A.S.K.

252 **FIGURE LEGENDS**

253 **Figure 1. Differential cell-to-cell variation in Hsf1 activity in response to heat shock and**
254 **AZC.**

255 **(A)** Anti-FLAG Western blot showing Hsf1 phosphorylation by electrophoretic mobility shift over
256 time in response to heat shock at 39ºC or 4 mM AZC.

257 **(B)** Hsf1 activity quantified by the levels of the HSE-YFP transcriptional reporter measured by
258 flow cytometry over time in response to heat shock at 39ºC or 4 mM AZC. The reporter consists
259 of four repeats of the heat shock element (HSE) recognized by Hsf1 upstream of a crippled
260 *CYC1* promoter. For each cell, the YFP level was normalized by side scatter (HSE-YFP/SSC) to
261 control for cell size. Each point represents the median of the fluorescence distribution of 10000
262 cells averaged over 3 biological replicates; error bars show the standard deviation of the
263 replicates.

264 **(C)** Single cell fluorescence distributions over a 4-hour heat shock time course. For each cell,
265 the YFP level was normalized by side scatter (HSE-YFP/SSC) to control for cell size.

266 **(D)** As in (C), but over a time course of treatment with 4 mM AZC.

267 **(E)** Overlay of the 4-hour time points from (C) and (D).

268 **(F)** Quantification of cell-to-cell variation in HSE-YFP/SSC levels over time courses in (C) and
269 (D) using the square of the coefficient of variation (CV^2) as a metric.

270

271 **Figure 2. Hsf1 phosphorylation generates cell-to-cell variation during heat shock.**

272 **(A)** Single cell fluorescence distributions over a heat shock time course in wild type cells and
273 cells expressing $Hsf1^{\Delta po4}$ as the only copy of Hsf1. For each cell, the YFP level was normalized
274 by side scatter (HSE-YFP/SSC) to control for cell size

275 **(B)** Quantification of cell-to-cell variation in HSE-YFP/SSC levels over time courses in (A).

276 **(C)** Images of wild type cells expressing the HSE-YFP reporter growing over time in a
277 microfluidic device at 25ºC and shifted to 39ºC at the indicated time. Scale bar is 10 μm.

278 **(D)** Quantification of HSE-YFP levels over time in the microfluidic device in wild type cells and
279 cells expressing Hsf1$^{\Delta po4}$ as the only copy of Hsf1. For each cell, the total YFP fluorescence was
280 divided by cell area to account for cell size differences. Each gray trace represents the trajectory
281 of a single cell and the thick lines show population averages.
282 **(E)** Quantification of cell-to-cell variation in HSE-YFP levels over time courses in (D).
283
284 **Figure 3. Cell-to-cell variation in Hsf1 activity promotes antifungal resistance in an**
285 **Hsp90-dependent manner.**
286 **(A)** Spinning disc confocal images of wild type cells and Hsf1$^{\Delta po4}$ cells expressing Hsp82-YFP.
287 Scale bar is 10 μm.
288 **(B)** Single cell fluorescence distributions of wild type cells and Hsf1$^{\Delta po4}$ cells expressing Hsp82-
289 YFP as determined by flow cytometry. For each cell, the YFP level was normalized by side
290 scatter (Hsp82-YFP/SSC) to control for cell size
291 **(C)** Appearance of fluconazole-resistant colonies in wild type cells and Hsf1$^{\Delta po4}$ cells. 10^6 cells
292 were plated on YPD plates supplemented with 128 μg/ml fluconazole and incubated at room
293 temperature for 4 days.
294 **(D)** Quantification of the number of fluconazole resistant colonies from three biological replicates
295 of the experiment shown in (C). Error bars show the standard deviation of the replicates (* $p < 0.05$; ** $p < 0.01$ by two-tailed T-test).
297 **(E)** Single cell fluorescence distributions of HSE-YFP/SSC in wild type and Hsp90 mutant cells.
298 under basal conditions. Deletion of *HSP82* leads to a modest increase in HSE-YFP levels, while
299 deletion of *HSC82* leads to a pronounced increase in HSE-YFP levels. The blue and red boxes
300 indicate the tails of the distribution with the highest and lowest expressing 10% of cells.
301 **(F)** Quantification of the number of fluconazole resistant colonies in the tails of the distributions
302 shown in (E) (* $p < 0.05$; ** $p < 0.01$ by two-tailed T-test).
303

304 **Figure 4. Fluconazole resistance correlates with cell-to-cell variation in Hsf1 activity.**

305 **(A)** Schematic showing the estradiol-inducible system used to titrate expression of wild type
306 Hsf1 and Hsf1$^{\Delta po4}$. A chimeric transcription factor containing the ligand binding domain of the
307 human estrogen receptor drives the expression of Hsf1 as a function of the concentration of
308 estradiol added to the growth media.

309 **(B)** Single cell HSE-YFP/SSC fluorescence distributions in cells treated across a dose response
310 of estradiol, ranging from 2-128 nM in cells expressing wild type Hsf1 (gray) or Hsf1$^{\Delta po4}$ (green)
311 as the only copy of Hsf1. Cells were incubated in log phase for 18 hours in the presence of the
312 indicated dose of estradiol to achieve steady state before measuring.

313 **(C)** Quantification of the median HSE-YFP/SSC across the estradiol dose response in wild type
314 and Hsf1$^{\Delta po4}$ cells relative to the maximum value.

315 **(D)** Quantification of the cell-to-cell variation (CV^2) of the HSE-YFP/SSC distributions across the
316 estradiol dose response in wild type and Hsf1$^{\Delta po4}$ cells.

317 **(E)** Overlays of the HSE-YFP/SSC distributions from wild type and Hsf1$^{\Delta po4}$ cells treated with the
318 indicated concentrations of estradiol.

319 **(F)** Quantification of fluconazole resistant colonies in wild type and Hsf1$^{\Delta po4}$ cells in the presence
320 of the indicated doses of estradiol (* $p < 0.05$; ** $p < 0.01$ by two-tailed T-test).

321 **(G)** Fluconazole resistant wild type and Hsf1$^{\Delta po4}$ colonies plotted as a function of median Hsf1
322 activity as measured by the HSE-YFP reporter. Dashed line is a linear regression to all six data
323 points showing a negative correlation.

324 **(H)** Fluconazole resistant wild type and Hsf1$^{\Delta po4}$ colonies plotted as a function of the variation in
325 Hsf1 activity as measured by the CV^2 of the HSE-YFP reporter. Dashed line is a linear
326 regression to all six data points showing a positive correlation.

327 **(I)** Correlation coefficients (r) of the data plotted in **(G)** and **(H)**.

328

329 **Figure S1. Characterization of the microfluidic heat shock device.**

330 **(A)** Schematic of the microfluidic heat shock device. The assembled device consists of a glass
331 coverslip patterned with Pt/Ti heater and sensor wires (grey), and a multilayer PDMS device
332 with flow (black and blue channels) and control (red channels) layers. Cells loaded from either
333 port A or B are trapped in chambers (blue) that have been fabricated to the height of a single
334 monolayer of *S. cerevisiae* cells. W denotes waste port.
335 **(B)** Representative calibration curve for the on-chip sensor showing a linear response across
336 the operating temperature range.
337 **(C)** Using the on-chip heater to achieve and accurately maintain chamber temperature of 39˚C,
338 as measured by a high-resolution long-wave infrared thermal camera.
339

340 **METHODS**

341 **Yeast strains and cell growth**

342 Yeast cells were cultured in SDC media as described (Zheng et al., 2016).

DPY number	Description	Genotype
144	WT HSE-YFP	W303 MATa 4xHSE-Venus::LEU
118	Hsf1-3xFLAG/V5	W303 MATa *hsf1*Δ::KAN Hsf1-3xFLAG-V5::TRP1
416	Hsf1Δpo4 HSE-YFP	W303 MATa *hsf1*Δ::KAN 4xHSE-Venus::LEU2 Hsf1Δpo4::TRP1
1221	hsc82Δ HSE-YFP	W303 MATa 4xHSE-Venus::LEU2 *hsc82*Δ::HYG
1222	hsp82Δ HSE-YFP	W303 MATa 4xHSE-Venus::LEU2 *hsp82*Δ::HYG

343

344 **Flow cytometry**

345 Flow cytometry was performed as described (Zheng et al., 2016). Data were processed in
346 FlowJo 10. Data were left ungated and YFP fluorescence was normalized by side scatter (SSC)
347 for each cell.

348

349 **Microfluidic heat shock time courses**

350 Single cell heat shock experiments were performed with a custom microfluidic device that uses
351 microscale, on-chip heaters to enable programmable thermal perturbations. The multilayer
352 device was fabricated out of the silicone elastomer polydimethylsiloxane (PDMS/Sylgard 184,
353 Dow Corning) using soft lithographic techniques, as described previously (Duffy et al., 1998;
354 Thorsen et al., 2002; Unger et al., 2000; Vega et al., 2012). The device was aligned and sealed
355 to a pre-cleaned No. 1.5 glass coverslip (Fisher Scientific), onto which micro-scale heater and
356 resistance temperature detector (RTD) wires were patterned. Briefly, a thin layer of Ti (100
357 Angstroms) was deposited on the glass, followed by a layer of Pt (150 nm) and finally a layer of
358 SPR 220-7 positive photoresist (MicroChem Corp.). After transferring the heater/RTD pattern to
359 the photoresist using a high-resolution transparency photomask (CAD/Art Services, Inc.), the
360 Pt/Ti layers were etched in Aqua Regia solution to generate the final serpentine pattern of

361 heater and RTD wires. The photoresist was then washed off with acetone, and a layer of SiO_2
362 (300 nm) was deposited on the final pattern. After assembly, the RTD of each device was
363 calibrated and confirmed to respond linearly to changes in the input temperature, as controlled
364 by a hot plate, across the operating temperature range of 25˚C to 45˚C (Figure S1). Additionally,
365 the devices were characterized by applying user-defined voltages to the heater and measuring
366 on-chip temperatures using a Flir A655sc high-resolution long-wave infrared thermal camera
367 (Flir Systems, Inc.) to validate the device's ability to achieve accurate and stable heat shock
368 conditions (Figure S1).
369
370 To perform microfluidic experiments, we used a custom microfluidic platform that controls the
371 delivery of liquids to the device and the actuation of valves (Vega et al., 2012). The voltage
372 across the heater wire and the resistance across the RTD wire were controlled and measured,
373 respectively, to modulate the on-chip temperature. For each experiment, cells were inoculated
374 1:100 from overnight SDC cultures into 2 mL SDC and allowed to grow 3-4 hours (OD ~0.5)
375 before seeding the device. Cells were then loaded into the device to trap a small number of cells
376 in growth chambers. Cells were grown on-chip in SDC media for 4-5 hours at 25˚C, ambient
377 conditions maintained with a Controlled Environment Microscope Incubator (Nikon Instruments,
378 Inc.) designed for live-cell imaging. Cells were then subjected to a heat shock by applying
379 voltage across the heater wire to ramp to and maintain an on-chip temperature of 39˚C.
380
381 Throughout, images were collected at 15-minute intervals at 100x magnification (Plan Apo
382 Lambda 100X, NA 1.45) using an Eclipse Ti-E inverted microscope (Nikon Instruments, Inc.)
383 equipped with the "Perfect Focus System", a XYZ-motorized stage, and a Clara-E charge-
384 coupled device (CCD) camera (Andor Technology). Images were acquired in phase contrast
385 configuration and in the YFP fluorescent channel. Filters and light sources (Nikon LED and
386 Lumencor SPECTRA X Light Engine) were automatically controlled using the supplier's

387 software (NIS-Elements Advanced Research). Following each experiment, cells were
388 segmented using custom image analysis software written for Matlab (Mathworks, Natick, MA),
389 and fluorescence values for each cell, averaged over cell area, were obtained from the time
390 series of YFP images.
391
392 **Spinning disc confocal imaging**
393 Imaging was performed as described (Zheng et al., 2016).
394
395 **Fluconazole acquired resistance assay**
396 Wild type and Hsf1$^{\Delta po4}$ cells were grown to mid-log phase and 10^6 cells were plated on YPD
397 plates with 128 µg/ml fluconazole + 25 nM estradiol. Plates were incubated for 4 days at room
398 temperature. Colonies were counted from 3 biological replicates and mean and standard
399 deviation were calculated.
400
401 **Fluorescence activated cell sorting**
402 10^6 cells from the high- and low-expressing tails (top and bottom 10% of cells) of the HSE-
403 YFP/SSC distribution in wild type, *hsp82*Δ and *hsc82*Δ cells were sorted in the Whitehead
404 Institute FACS facility on a BD FACS Aria.
405
406 **Estradiol dose responses**
407 Performed as described (Zheng et al., 2016).
408
409
410

411 **REFERENCES**

412 Anckar, J., and Sistonen, L. (2011). Regulation of HSF1 function in the heat stress response:
413 implications in aging and disease. Annu Rev Biochem *80*, 1089-1115.

414 Colman-Lerner, A., Gordon, A., Serra, E., Chin, T., Resnekov, O., Endy, D., Pesce, C.G., and
415 Brent, R. (2005). Regulated cell-to-cell variation in a cell-fate decision system. Nature *437*, 699-
416 706.

417 Cowen, L.E., and Lindquist, S. (2005). Hsp90 potentiates the rapid evolution of new traits: drug
418 resistance in diverse fungi. Science *309*, 2185-2189.

419 Duffy, D.C., McDonald, J.C., Schueller, O.J., and Whitesides, G.M. (1998). Rapid Prototyping of
420 Microfluidic Systems in Poly(dimethylsiloxane). Anal Chem *70*, 4974-4984.

421 Elowitz, M.B., Levine, A.J., Siggia, E.D., and Swain, P.S. (2002). Stochastic gene expression in
422 a single cell. Science *297*, 1183-1186.

423 Fowden, L., and Richmond, M.H. (1963). Replacement of Proline by Azetidine-2-Carbolic Acid
424 during Biosynthesis of Protein. Biochim Biophys Acta *71*, 459-&.

425 Harms, A., Maisonneuve, E., and Gerdes, K. (2016). Mechanisms of bacterial persistence
426 during stress and antibiotic exposure. Science *354*.

427 Newman, J.R., Ghaemmaghami, S., Ihmels, J., Breslow, D.K., Noble, M., DeRisi, J.L., and
428 Weissman, J.S. (2006). Single-cell proteomic analysis of S. cerevisiae reveals the architecture
429 of biological noise. Nature *441*, 840-846.

430 Oderberg, I.M., Li, D.J., Scimone, M.L., Gavino, M.A., and Reddien, P.W. (2017). Landmarks in
431 Existing Tissue at Wounds Are Utilized to Generate Pattern in Regenerating Tissue. Curr Biol
432 *27*, 733-742.

433 Queitsch, C., Sangster, T.A., and Lindquist, S. (2002). Hsp90 as a capacitor of phenotypic
434 variation. Nature *417*, 618-624.

435 Raj, A., and van Oudenaarden, A. (2008). Nature, nurture, or chance: stochastic gene
436 expression and its consequences. Cell *135*, 216-226.

437 Raser, J.M., and O'Shea, E.K. (2004). Control of stochasticity in eukaryotic gene expression.
438 Science *304*, 1811-1814.

439 Raser, J.M., and O'Shea, E.K. (2005). Noise in gene expression: origins, consequences, and
440 control. Science *309*, 2010-2013.

441 Rodina, A., Wang, T., Yan, P., Gomes, E.D., Dunphy, M.P., Pillarsetty, N., Koren, J.,
442 Gerecitano, J.F., Taldone, T., Zong, H.*, et al.* (2016). The epichaperome is an integrated
443 chaperome network that facilitates tumour survival. Nature *538*, 397-401.

444 Rutherford, S.L., and Lindquist, S. (1998). Hsp90 as a capacitor for morphological evolution.
445 Nature *396*, 336-342.

446 Sangster, T.A., Lindquist, S., and Queitsch, C. (2004). Under cover: causes, effects and
447 implications of Hsp90-mediated genetic capacitance. Bioessays *26*, 348-362.

448 Serio, T.R., and Lindquist, S.L. (1999). [PSI+]: an epigenetic modulator of translation
449 termination efficiency. Annu Rev Cell Dev Biol *15*, 661-703.

450 Shorter, J., and Lindquist, S. (2005). Prions as adaptive conduits of memory and inheritance.
451 Nat Rev Genet *6*, 435-450.

452 Shorter, J., and Lindquist, S. (2008). Hsp104, Hsp70 and Hsp40 interplay regulates formation,
453 growth and elimination of Sup35 prions. EMBO J *27*, 2712-2724.

454 Silva, J., and Smith, A. (2008). Capturing pluripotency. Cell *132*, 532-536.

455 Solis, E.J., Pandey, J.P., Zheng, X., Jin, D.X., Gupta, P.B., Airoldi, E.M., Pincus, D., and Denic,
456 V. (2016). Defining the Essential Function of Yeast Hsf1 Reveals a Compact Transcriptional
457 Program for Maintaining Eukaryotic Proteostasis. Mol Cell *63*, 60-71.

458 Stelzer, Y., Shivalila, C.S., Soldner, F., Markoulaki, S., and Jaenisch, R. (2015). Tracing
459 dynamic changes of DNA methylation at single-cell resolution. Cell *163*, 218-229.

460 Stewart-Ornstein, J., Weissman, J.S., and El-Samad, H. (2012). Cellular noise regulons underlie
461 fluctuations in Saccharomyces cerevisiae. Mol Cell *45*, 483-493.

462 Thorsen, T., Maerkl, S.J., and Quake, S.R. (2002). Microfluidic large-scale integration. Science
463 *298*, 580-584.

464 Trotter, E.W., Kao, C.M., Berenfeld, L., Botstein, D., Petsko, G.A., and Gray, J.V. (2002).
465 Misfolded proteins are competent to mediate a subset of the responses to heat shock in
466 Saccharomyces cerevisiae. J Biol Chem *277*, 44817-44825.

467 Unger, M.A., Chou, H.P., Thorsen, T., Scherer, A., and Quake, S.R. (2000). Monolithic
468 microfabricated valves and pumps by multilayer soft lithography. Science *288*, 113-116.

469 Vega, N.M., Allison, K.R., Khalil, A.S., and Collins, J.J. (2012). Signaling-mediated bacterial
470 persister formation. Nat Chem Biol *8*, 431-433.

471 Weinberger, L.S., Burnett, J.C., Toettcher, J.E., Arkin, A.P., and Schaffer, D.V. (2005).
472 Stochastic gene expression in a lentiviral positive-feedback loop: HIV-1 Tat fluctuations drive
473 phenotypic diversity. Cell *122*, 169-182.

474 Ye, X., and Weinberg, R.A. (2015). Epithelial-Mesenchymal Plasticity: A Central Regulator of
475 Cancer Progression. Trends Cell Biol *25*, 675-686.

476 Zheng, X., Krakowiak, J., Patel, N., Beyzavi, A., Ezike, J., Khalil, A.S., and Pincus, D. (2016).
477 Dynamic control of Hsf1 during heat shock by a chaperone switch and phosphorylation. Elife *5*.
478

Figure 1

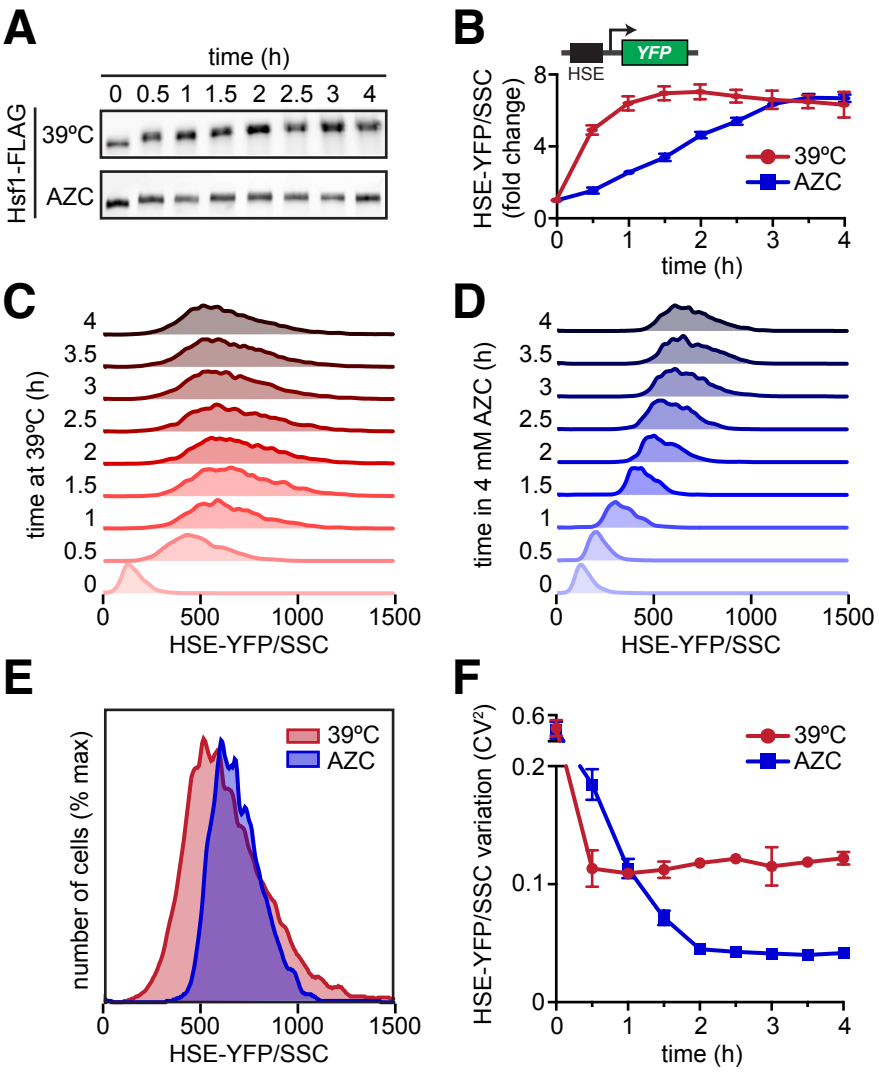
A
time (h)
0 0.5 1 1.5 2 2.5 3 4
Hsf1-FLAG
39ºC
AZC
B
HSE
YFP
HSE-YFP/SSC (fold change)
39ºC
AZC
time (h)
C
time at 39ºC (h)
HSE-YFP/SSC
D
time in 4 mM AZC (h)
HSE-YFP/SSC
E
number of cells (% max)
39ºC
AZC
HSE-YFP/SSC
F
HSE-YFP/SSC variation (CV²)
39ºC
AZC
time (h)

Figure 2

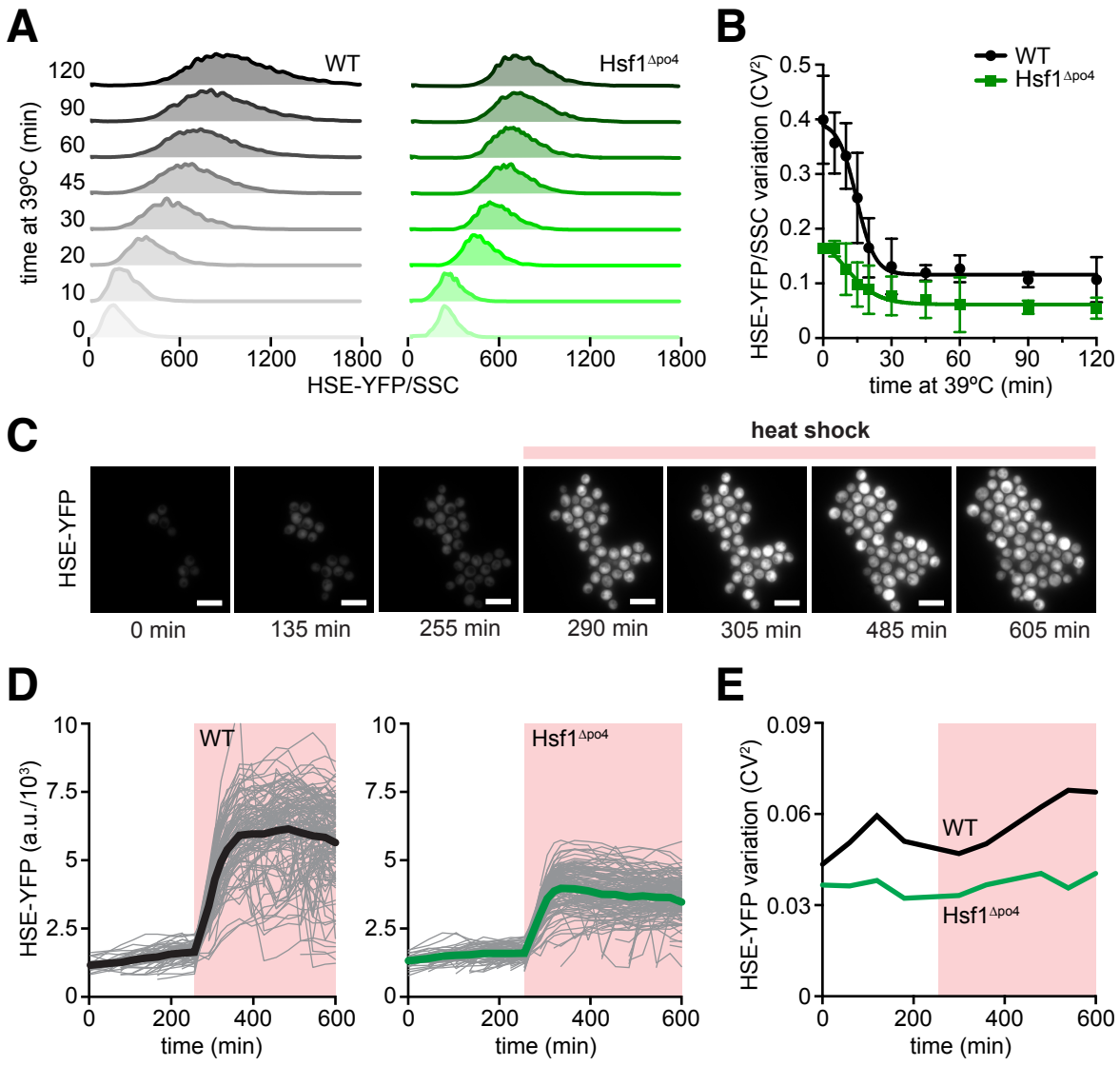
A
WT
Hsf1Δpo4
time at 39ºC (min)
120
90
60
45
30
20
10
0
0
600
1200
1800
HSE-YFP/SSC
B
WT
Hsf1Δpo4
HSE-YFP/SSC variation (CV²)
0.5
0.4
0.3
0.2
0.1
0
30
60
90
120
time at 39ºC (min)
C
heat shock
HSE-YFP
0 min
135 min
255 min
290 min
305 min
485 min
605 min
D
WT
Hsf1Δpo4
HSE-YFP (a.u./10³)
10
7.5
5
2.5
0
200
400
600
time (min)
E
HSE-YFP variation (CV²)
0.09
0.06
0.03
WT
Hsf1Δpo4
time (min)

Figure 3

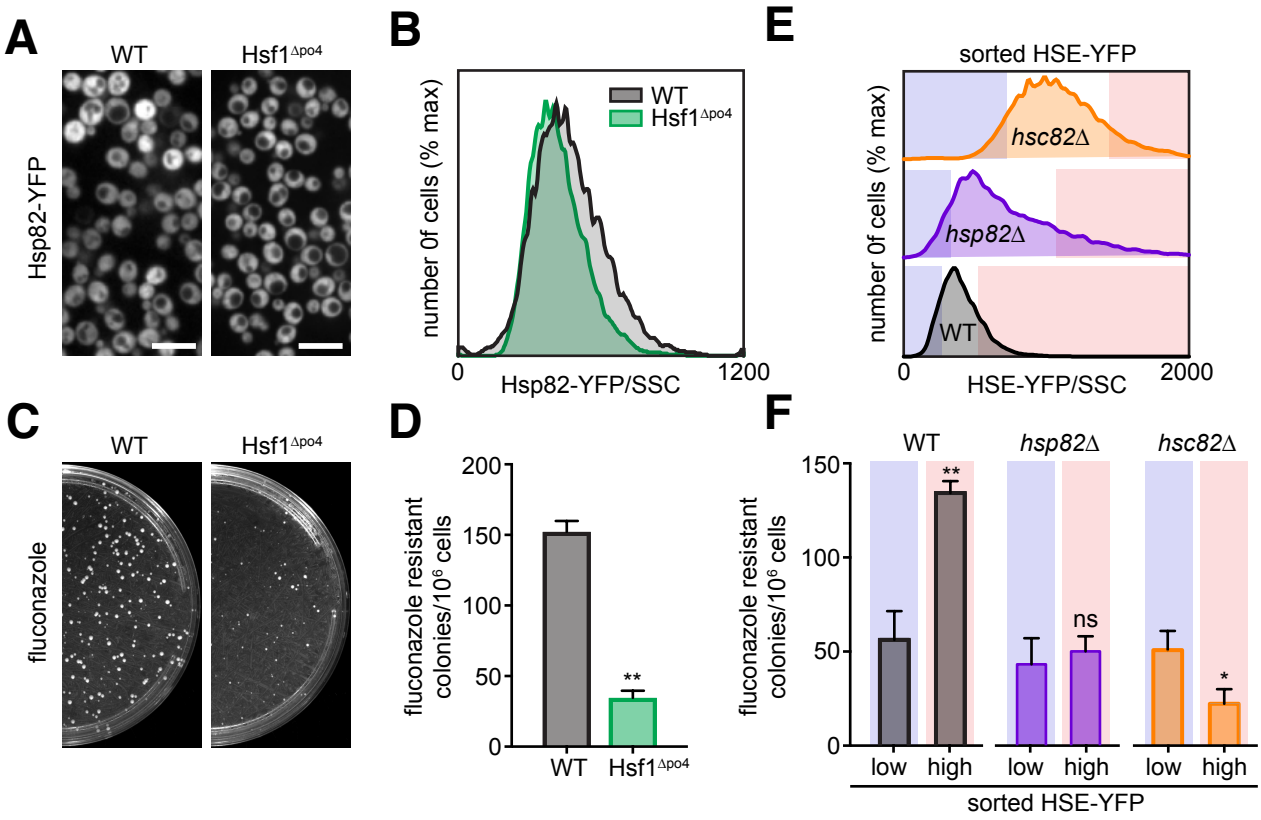
A
WT
Hsf1Δpo4
Hsp82-YFP
B
WT
Hsf1Δpo4
number 0f cells (% max)
0
1200
Hsp82-YFP/SSC
E
sorted HSE-YFP
hsc82Δ
hsp82Δ
WT
number 0f cells (% max)
0
2000
HSE-YFP/SSC
C
WT
Hsf1Δpo4
fluconazole
D
fluconazole resistant colonies/10^6 cells
200
150
100
50
0
**
WT
Hsf1Δpo4
F
WT
hsp82Δ
hsc82Δ
fluconazole resistant colonies/10^6 cells
150
100
50
0
**
ns
*
low
high
low
high
low
high
sorted HSE-YFP

Figure 4

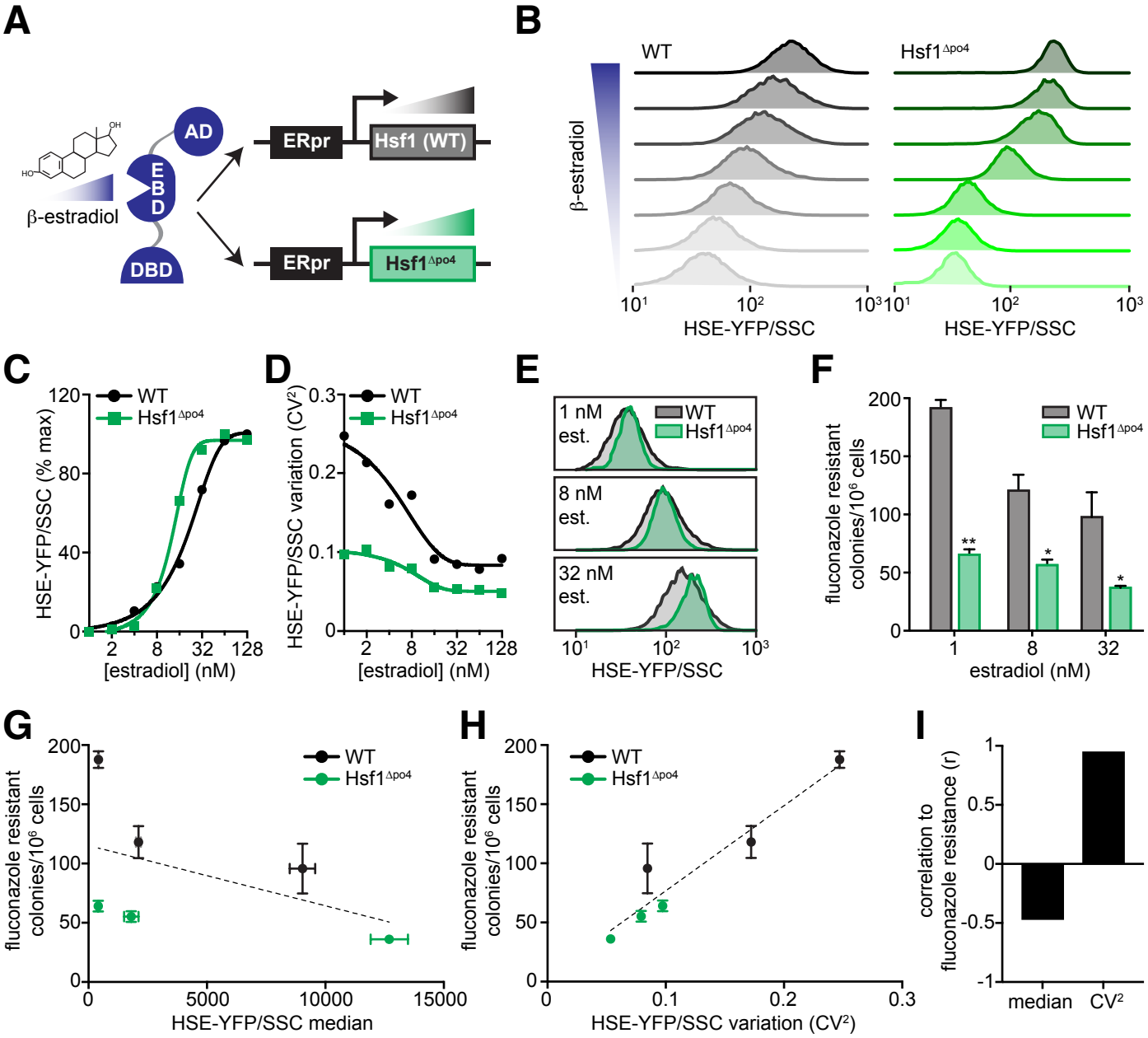
A
AD
EBD
DBD
β-estradiol
ERpr
Hsf1 (WT)
ERpr
Hsf1Δpo4
B
WT
Hsf1Δpo4
β-estradiol
HSE-YFP/SSC
HSE-YFP/SSC
C
WT
Hsf1Δpo4
HSE-YFP/SSC (% max)
[estradiol] (nM)
D
WT
Hsf1Δpo4
HSE-YFP/SSC variation (CV²)
[estradiol] (nM)
E
1 nM est.
8 nM est.
32 nM est.
WT
Hsf1Δpo4
HSE-YFP/SSC
F
WT
Hsf1Δpo4
fluconazole resistant colonies/10⁶ cells
estradiol (nM)
G
WT
Hsf1Δpo4
fluconazole resistant colonies/10⁶ cells
HSE-YFP/SSC median
H
WT
Hsf1Δpo4
fluconazole resistant colonies/10⁶ cells
HSE-YFP/SSC variation (CV²)
I
correlation to fluconazole resistance (r)
median
CV²

Figure S1

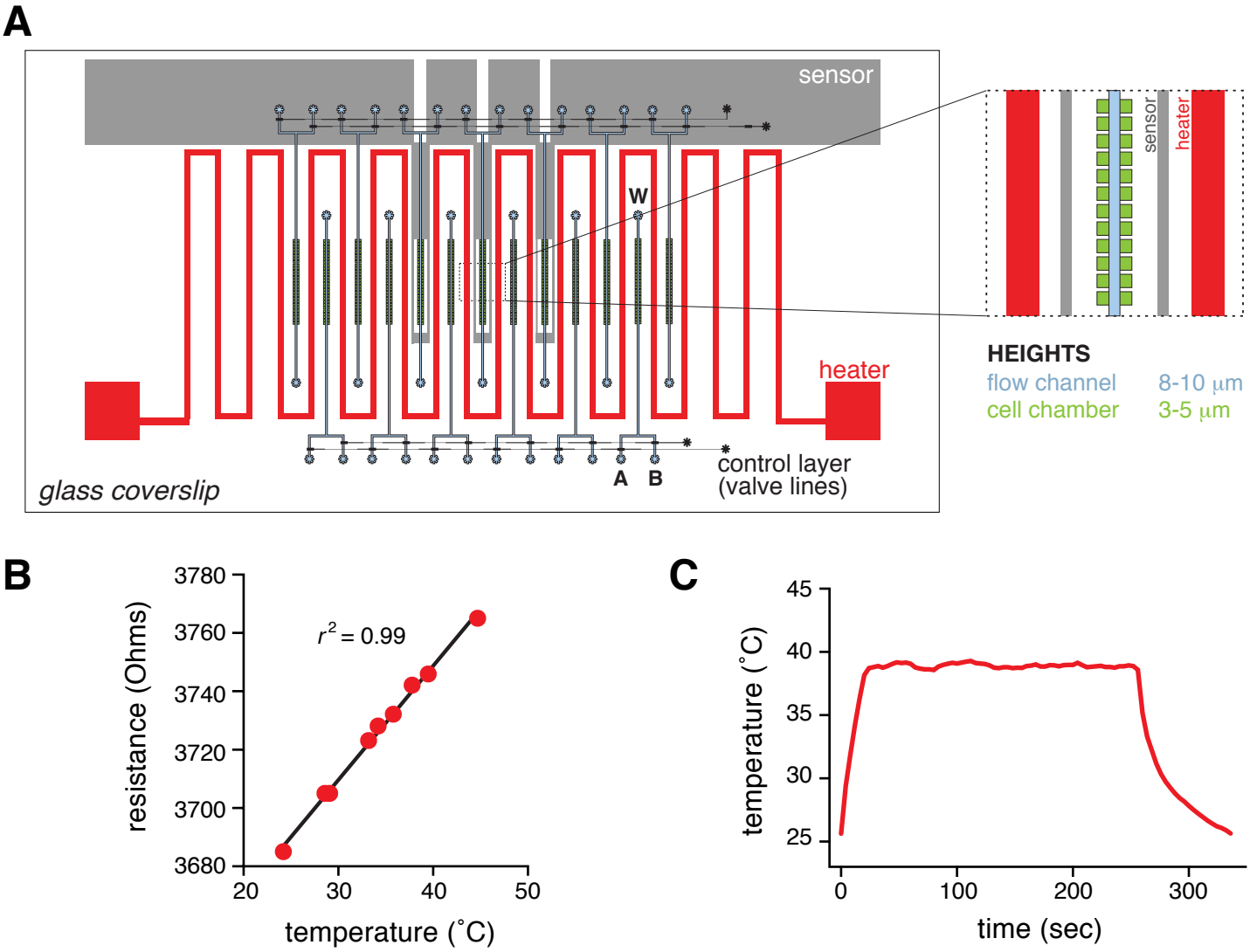
A
sensor
W
heater
A
B
control layer
(valve lines)
glass coverslip
sensor
heater
HEIGHTS
flow channel
8-10 μm
cell chamber
3-5 μm
B
resistance (Ohms)
3780
3760
3740
3720
3700
3680
$r^2 = 0.99$
20
30
40
50
temperature (˚C)
C
temperature (˚C)
45
40
35
30
25
0
100
200
300
time (sec)